AIAA SciTech Forum
8-12 January 2024, Orlando, FL
AIAA SCITECH 2024 Forum

10.2514/6.2024-1031

300 kHz OH PLIF of Detonation Structure

Mark D. Frederick*[1], Ryan M. Strelau†[1], Rohan M. Gejji‡[1], Joseph E. Shepherd§[2], and Carson D. Slabaugh¶[1]
[1]*Purdue University, West Lafayette, IN 47907*
[2]*California Institute of Technology, Pasadena, CA 91125*

The reaction field within detonations of methane-oxygen-nitrogen and hydrogen-oxygen-nitrogen are imaged with OH planar laser induced fluorescence (PLIF) at a rate of 300 kHz. Simultaneously, 5 MHz schlieren and broadband chemiluminescence measurements are acquired. The OH PLIF and chemiluminescence images are compared and small-scale structures are resolvable with the PLIF that are otherwise integrated over in the chemiluminescence. In the methane fueled mixture, an asymmetric transverse wave collision is analyzed and by overlaying the schlieren and PLIF images, localized reaction is observed within vortices ejected from the symmetry line of the collision. In a hydrogen fueled mixture, a Kelvin-Helmholtz instability is resolved along the shear layer between the high-speed shock and transverse wave. The OH PLIF signal tightly conforms to the vortices on the high-speed shock side of the shear layer. The formation of an unreacted gas pocket is captured and as the pocket convects downstream increased OH PLIF emission around the periphery suggests that it burns deflagratively.

I. Introduction

The intrinsic instability of gaseous detonation waves manifests as an oscillating lead shock with associated weaker shocks moving laterally, relative to the front. This unsteady flow state is accompanied by a coupled and concomitantly unsteady reaction zone. Each field, the gas-dynamic and chemical-kinetic, requires a separate diagnostic to properly resolve. In 1961, White [1] was the first to study the structure of the wave using interferometry. With the discovery of the cellular instability, soot foils became [2, 3] and have remained [4, 5] a popular approach to record the history of the wave front. In narrow channels designed to suppress the third dimension of this instability, which would otherwise confuse interpretation with a path-integrated diagnostic, schlieren and shadowgraph imaging have become the standard techniques to resolve the gas-dynamic field. Initially only single-shot [6–8] or short high-speed movies [9–11] could be acquired due to restrictions imposed by the diagnostic equipment. More recently, and owing to advancements in high-speed CMOS and LED technology, schlieren images have been acquired at rates $O(100\ \text{kHz})$ that enable the dynamic evolution of flow structure to be temporally resolved [12–16]. By pulsing an LED at 5 MHz, Frederick *et al.* [17] have been able to measure and statistically describe the velocity oscillation of the leading front.

Early investigators relied on open-shutter photography of the self-luminosity of the detonation to image the reaction zone [6, 18, 19]. Like soot foils, this technique captures the spatial history of the reaction zone, but is not temporally resolved. Using modern high-speed and intensified cameras time-resolved self-luminous (broadband) and filtered chemiluminescence images have been acquired in conjunction with schlieren to study the coupled fields [11, 15, 17, 20–22]. Chemiluminescence imaging is extremely useful due to its ease of execution and the ability to record at MHz repetition rates [17]. However, the recorded signal intensity is dependent on the emitted light from the detonation, the selected spectral filter (if any), the mixture composition, and the integration time of the sensor ($O(100\ \text{ns})$).

An alternative technique used to characterize the detonation reaction zone structure is planar laser induced fluorescence (PLIF). As compared to chemiluminescence, PLIF has a number of benefits. When performing PLIF a specific molecule is excited to a higher electronic level with a laser pulse tuned to a precise absorption transition. The resulting spontaneous emission is often of much greater intensity than the natural chemiluminescence, which enables a shorter imaging integration time ($O(20\ \text{ns})$). Signal is only generated within the plane formed by the thin laser sheet and path-integration effects are minimized. The generated signal is also linear with incident laser intensity, so in theory to produce more signal only a more powerful laser is required. In practice, this is often difficult to achieve.

*Graduate Research Assistant, School of Mechanical Engineering, AIAA Student Member
†Graduate Research Assistant, School of Aeronautics and Astronautics, AIAA Student Member
‡Senior Research Engineer, School of Aeronautics and Astronautics, AIAA Senior Member
§C. L."Kelly" Johnson Professor of Aeronautics and Mechanical Engineering, Graduate Aerospace Laboratories
¶Paula Feuer Associate Professor, School of Aeronautics and Astronautics, AIAA Associate Fellow

Single-shot OH PLIF has been performed by Austin *et al.* [10, 23] to study the reaction zone structure within mixtures of varying instability. It was determined that distortion in the OH front increases with mixture instability. Comparing with some of the cases in [10], Mével *et al.* [24] developed a LIF model to extract qualitative information from the images. Using the same system as Austin [25], Pintgen and Shepherd [21] studied the influence of the cellular instability on the process of detonation diffraction. More recently, Rojas Chavez *et al.* [26] performed single-shot OH PLIF in mixtures of hydrogen-air and varied the laser wavelength to evaluate various excitation lines.

Aside from obtaining spatial information about the location of the reaction zone, it is also possible to use PLIF to obtain quantitative information. Single-shot measurements of the equilibrium temperature behind hydrogen-air mixtures initiated at atmospheric pressure were recently demonstrated using two-color OH PLIF [27]. By seeding mixtures of hydrogen-air with NO, Rojas Chavez *et al.* [28] used NO PLIF to make single-shot measurements of the induction zone length behind the leading shock.

In this work we apply 300 kHz OH PLIF in a narrow detonation channel to study the conception and evolution of key features within the reaction zone of methane-oxygen-nitrogen and hydrogen-oxygen-nitrogen mixtures. Simultaneously obtained 5 MHz schlieren allows for these features to be discussed in the context of the coupled gas-dynamic field. Observations are made regarding the consumption of reactants by turbulent mechanisms and the fate of unreacted gas pockets that persist downstream of the leading front.

II. Experiment Description

A. Detonation Channel

The *Narrow Channel Facility* (NCF) was developed by Austin[23] in the Explosion Dynamics Laboratory at Caltech to study the unstable structure in gaseous detonations. The NCF is a high aspect ratio, rectangular channel with a height of 152.4 mm width of 17.8 mm, and span of 4.2 m. The dimensions were chosen such that the width is nominally smaller than the detonation cell size for a targeted range of mixtures and test conditions. This configuration effectively suppresses transverse wave motion across the width of the channel, generating a two-dimensional detonation structure across the channel height that is conducive to the application of path-integrated optical diagnostics.

The reactant gases, typically an oxidizer, an inert, and one or two fuels, are introduced into the channel using the method of partial pressures. The loading process takes approximately 120 seconds and the reactants are circulated for an additional thirty seconds to ensure a homogeneous mixture. A K-type thermocouple and low frequency pressure transducer are used to record the initial temperature and pressure. The planar detonation is driven by a branched initiator, designed by Jackson and Shepherd [29]. The initiator operates with an equimolar C_2H_2-O_2 mixture and is ignited with a spark plug. The facility is operated at low pressure ($\approx$ 20 kPa) to produce large structures that are amenable to observation with imaging diagnostics.

Pressure fluctuations in the channel are recorded at six axially distributed locations using PCB 113B26 high-frequency dynamic pressure transducers (PT), installed flush with the channel wall, and sampled at 3.5 MHz. PT 1-3 monitor the planarity of the wave as it enters the test section. PT 4-8 are used to track the progression of the detonation wave as it traverses the channel by using the time of arrival method. These data can be used to monitor the detonation velocity and compare with the theoretical Chapman Jouguet velocity. Figure 1 identifies the location of all the high-frequency pressure measurement locations (PT 1-8). More details on the experimental procedure are available in Frederick *et al.* [15, 30].

B. Diagnostics

Schlieren, broadband chemiluminescence, and OH planar laser induced fluorescence were performed simultaneously in this work. All utilized the optical access provided by 170 mm fused quartz windows located at the end of the channel, shown in Figure 1. All cameras are placed on the same side of the experiment and image through the same window.

1. Schlieren

Schlieren was performed in a lens-type configuration with a pulsed LED light-source. The LED produced incoherent 635 ± 7 nm light with a 110 ns pulse duration at a 5 MHz pulse frequency. An aspheric condenser lens was placed directly downstream of the LED and passed the focus of the beam through an aperture to enforce a point source. A 250 mm lens was used to collimate the light through the test section and a 500 mm lens was used to collect the light and focus it onto the schlieren cutoff, which was a circular aperture. To eliminate emission from the detonation from reaching the

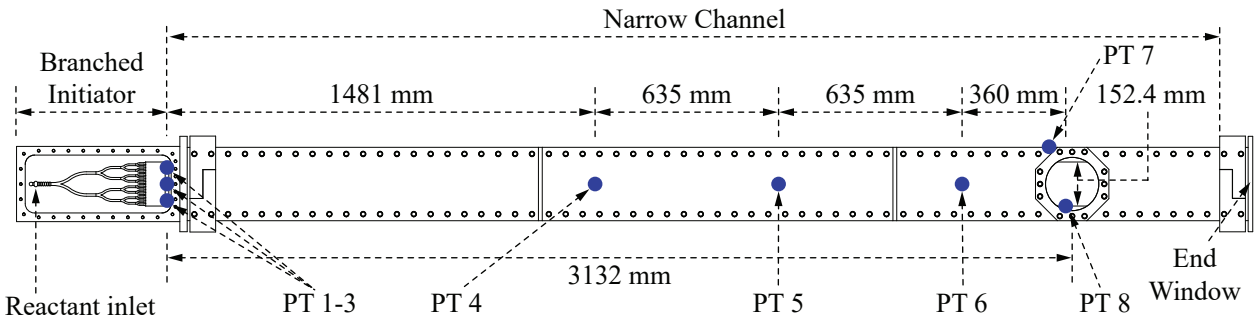

Fig. 1 Experimental overview and dimensions. High-frequency pressure measurement locations labeled as PT 1-8.

camera, the light passed through a 631/21 nm single-band bandpass filter. 128 images were record at a rate of 5 MHz on a Shimadzu HPV-X2 high-speed camera with a 150 mm custom camera lens. The Shimadzu HPV-X2 detector has a sensor size of 400 x 250 pixels. The field of view was 54.8 x 34.2 mm, yielding a spatial resolution of 137 μm/px.

2. Chemiluminescence

A second Shimadzu HPV-X2 was used to record the broadband chemiluminescence emission of the detonation. This camera was placed above the schlieren beam path and angled downwards at nine degrees to achieve a coincident field of view with the schlieren camera. The resulting image perspective was corrected for in Davis 10.2.1. The clocks of the two HPV-X2's were synchronized so that recording occurred simultaneously. The frame rate, exposure time, and field of view all match the schlieren configuration.

3. Planar laser-induced fluorescence

The OH PLIF system consisted of a flash-lamp pumped, Nd:YAG burst-mode laser (BML) (Spectral Energies QuasiModo) and an optical parametric oscillator (OPO). The BML produced a short burst of high-energy pulses at 300 kHz and with a 10 ns pulse width, shown in Figure 2. The duration of the pulse train was limited to what was needed to resolve the wave passage through the field of view. The frequency-doubled (532 nm) and -tripled (355 nm) output of the BML provided 40 mJ/pulse and 80 mJ/pulse, respectively.

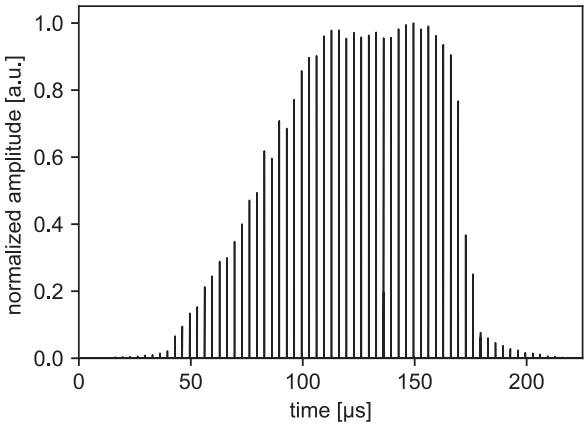

Fig. 2 Output of pulse burst laser at 300 kHz repetition rate.

The OPO was pumped in a double-pass configuration with the 355 nm output of the BML [31]. The OPO consisted of a pair of un-coated, manually tuned Type-I beta-barium-borate (BBO) crystals that were 15 mm long and cut at 32.8°. The cavity was tuned to a signal wavelength of ≈609 nm and injection seeded with an external cavity diode laser (Sacher, Lion) at an idler wavelength of ≈850 nm to narrow the signal line-width. Only the signal beam was resonant in the cavity.

The OPO produced about 14 mJ/pulse at the signal wavelength and was then mixed with the 532 nm output of the BML in a BBO crystal cut at 43° (sum-frequency-generation) to produce a ≈284 nm beam with an energy of 0.9 mJ/pulse.

Due to the large jump in pressure across the detonation wave and the uncertainty in thermodynamic properties and mixture composition, selection of a specific narrow band absorption line was avoided. Instead, the OPO and SFG crystals and idler laser were tuned to produce a system output frequency between the $Q_1(9)$ and $Q_2(8)$ lines of the $A^2\Sigma^+(v' = 1) \leftarrow X^2\Pi(v'' = 0)$ transitions. Figure 3 shows excitation LIF profiles computed with LIFBASE 2.1.1 [32] for a representative thermodynamic state within a hydrogen, oxygen, nitrogen detonation (cases B and C in Table 1). All parameters are the same in the two profiles, except that collisional broadening is not included in (a) and it is included in (b). The modeling parameters are: P = 5 atm, T = 2000 K, $\Delta\lambda_{Doppler}$ = 2.20 pm, $\Delta\lambda_{collisional}$ = 3.69 pm, $\delta\lambda_{collisional}$ = 1.0 pm, $\delta\lambda_{Doppler}$= -1.0 pm. The product gas composition is assumed to be 30% H_2O and 70% N_2 because limited data is available for the spectroscopic parameters of the minor species. The collisional and Doppler line broadening and shifting values are computed according to the equations provided in Hanson *et al.* [33]. The collisional broadening and shift coefficients are estimated from the experimental measurements of Rea *et al.* [34] and Kessler *et al.* [35], respectively. The blue dotted line represents that target wavelength, 284.007 nm, to which the laser system was tuned. A wavelength meter (HighFinesse WS6-200) was used to measure the wavelength of the idler and BML fundamental to ensure the target wavelength was reached. Upon passage of the detonation wave, the pressure behind the front will increase causing the $Q_1(9)$ and $Q_2(8)$ lines to broaden into each other. Even if the other broadening/shift terms change due to changing flow properties, the broad peak should still encompass the excitation wavelength.

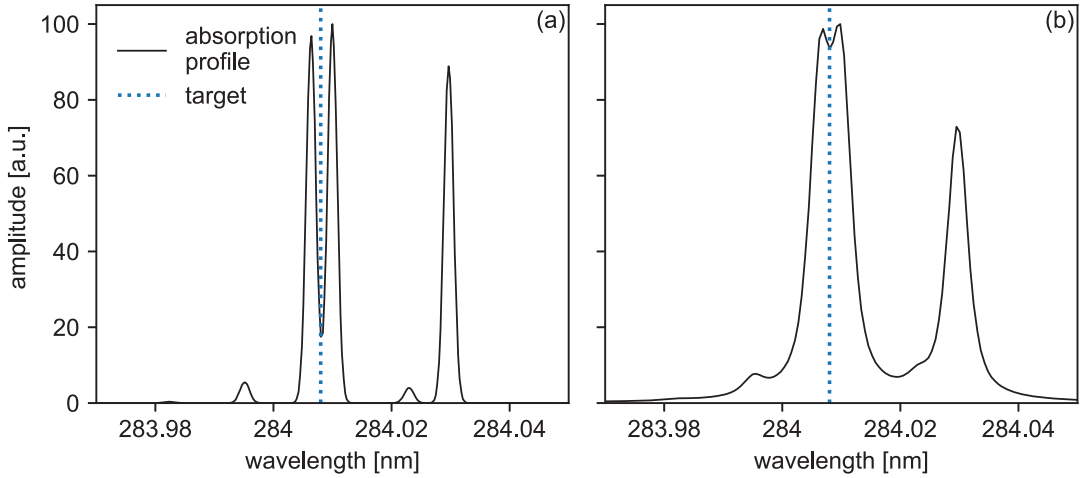

Fig. 3 Absorption profile (a) not including pressure broadening and (b) including pressure broadening.

A series of cylindrical lenses was used to transform the 284 nm beam into a collimated sheet about 46 mm tall. The sheet was focused into the test section (in the depth direction) using a cylindrical lens with f = 750 mm and entered the experiment through a fused-quartz window fixed to the end-flange (see Fig.1). The OH PLIF signal was collected with a f = 100 mm UV grade objective lens with f/2.8 (Cerco). A dual-stage multi-channel plate image intensifier (HiCATT 25 S20) was used to amplify and temporally gate (20 ns) the signal. The image was recorded on a Phantom TMX-7510 operating at 300 kHz, in binned mode, and with a sensor size of 640 x 384 px. The field of view imaged was 93 x 57 mm, yielding a spatial resolution of 145 μm/px. The fluorescence signal, expected between 305 - 320 nm ($A^2\Sigma^+(v' = 1) \rightarrow X^2\Pi(v'' = 1)$ and $A^2\Sigma^+(v' = 0) \rightarrow X^2\Pi(v'' = 0)$), was spectrally filtered with a 313/10nm band-pass filter (Edmund 34-981). The entire collection setup (camera, intensifier, lens, filter) was placed beneath the schlieren beam path and angled up at 12° to have a coincident field of view with the schlieren and chemiluminescence. A perspective transform was again performed.

Placed immediately upstream of the end-flange window was a UV beam sampler (Thorlabs BSF20-UV) that reflected about 8% of the incident laser sheet onto a white piece of printer paper. The fluorescence produced on the paper was imaged at a resolution of 768x80 on a Phantom v2512 that synchronously recorded with the TMX-7510. To prevent saturation of the camera sensor, neutral density filters totaling OD = 2.1 were placed in front of the camera lens. All pixels in a row were summed to produce the 1D trace in Fig. 4. Additionally, the 1D traces of all pulses from a single burst are shown in Figure 5. There is a clear shot-to-shot variation in both beam profile and intensity.

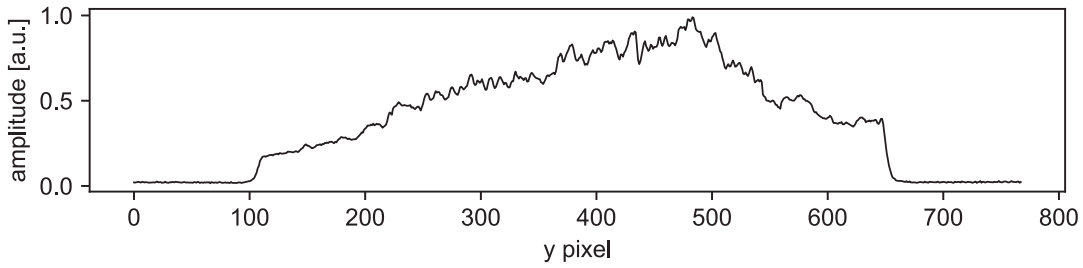

Fig. 4 1D trace computed by summing over all pixels at a given y-location of fluorescence on white paper.

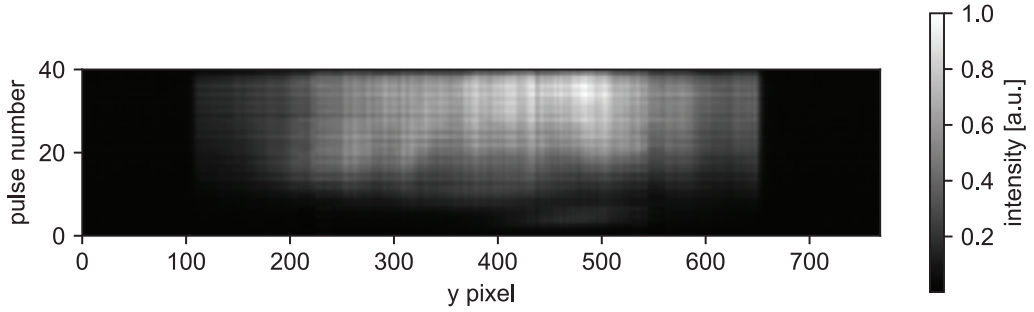

Fig. 5 Laser sheet profile of consecutive pulses normalized by the maximum pixel intensity.

The PLIF signal is linear with respect to excitation energy and the beam profile non-uniformity must be taken into account to ensure a correct interpretation of the resulting images. The 1D sampled intensity profiles from each shot are smoothed and normalized by the maximum pixel intensity for a case and then divided from each row of the corresponding PLIF image. Three sample images in Figure 6 show the results of the correction. In the left column (a,c,e) are the original images and in the right column are the corrected images (b,d,f). In comparing (a) and (b), the top most section of the low-speed shock in (a) is dark, but once the correction is applied in (b) that feature is restored. By boosting the signal in this manner, a requisite increase in noise is also apparent. In frames (e) and (f), the bright portion of the low-speed shock is reduced once the correction is applied. As the images progress forward in time (a $\rightarrow$ c $\rightarrow$ e) the total laser pulse energy increases (see Fig. 5) and image (a) appears darker than (e). Once the correction is applied, this trend is eliminated and the images in (b), (d), and (f) can be faithfully compared.

III. Results

Three cases of two different mixtures will be examined in the subsequent section. Case (A) is a mixture of stoichiometric methane and oxygen diluted with 37.5% nitrogen and cases (B) and (C) are mixtures of stoichiometric hydrogen and oxygen diluted with 57% nitrogen. These cases are listed in Table 1 along with the initial pressures and temperatures (P_0 and T_0) and the detonation properties computed with the ZND equations [36]. Note that the hydrogen cases (B and C) were all propagating at about $0.9U_{CJ}$ when approaching the window section. This results in a spatial structure that is larger and less regular than what is normally expected for this mixture.

Table 1 Calculated detonation parameters. P_{vN} and T_{vN} are the von Neumann pressure and temperature. U_{CJ} is the Chapman-Jouguet velocity, Δ_I is the induction length, Δ_E is the exothermic length, and θ is the non-dimensional activation energy. All parameters are found using the Shock and Detonation Toolbox [36] with the GRI3.0 reaction mechanism [37].

Case	P_0 [kPa]	T_0 [K]	PvN [kPa]	T_{vN} [K]	U_{CJ} [m/s]	Δ_I [mm]	Δ_E [μm]	θ
A	26	302	1,081	1711	2084	3.64	137	11.6
B, C	29	300	769	1492	1929	0.71	196	5.6

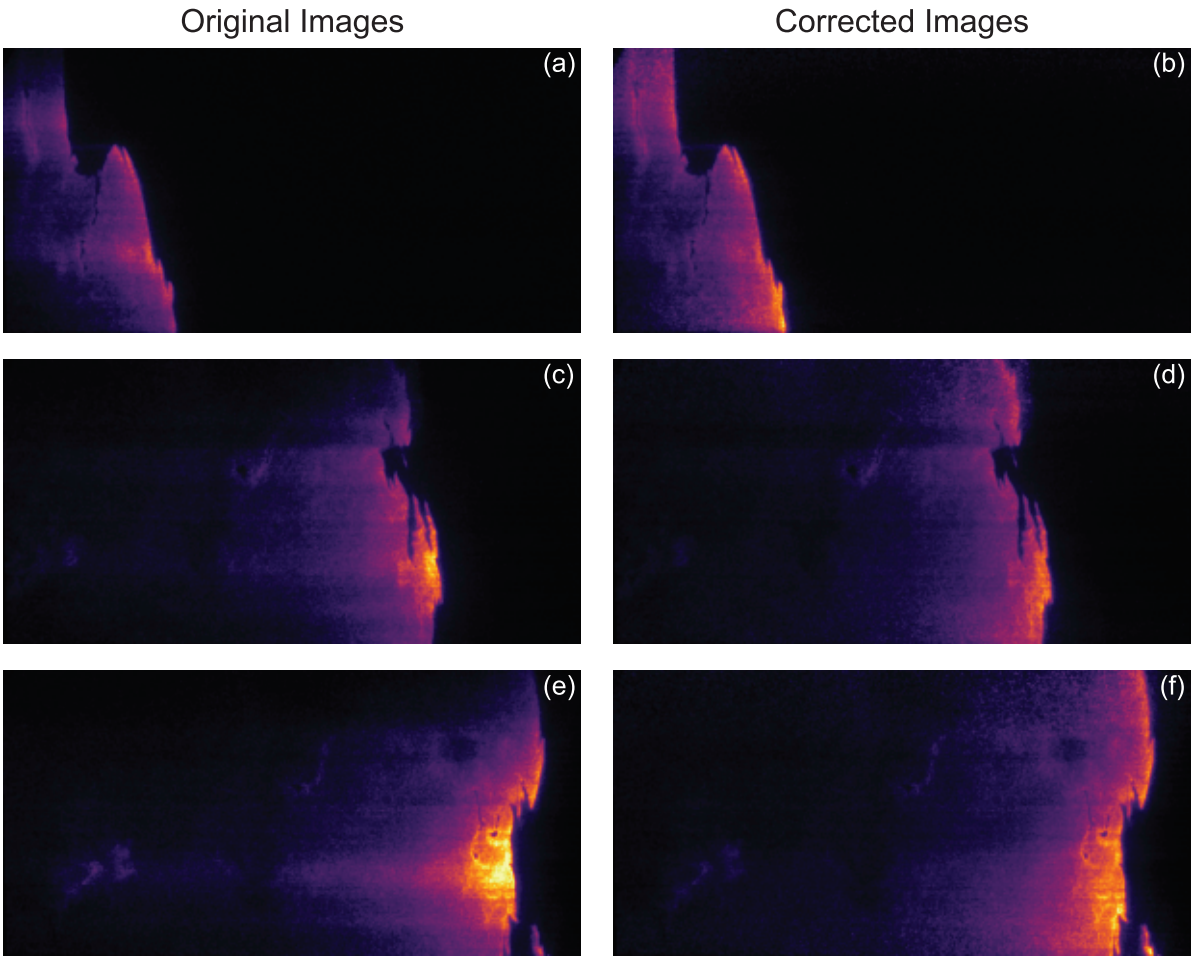

Fig. 6 Original PLIF images (a,c,e) and the same images with the sheet profile correction applied (b,d,f).

A. Comparison of OH PLIF and chemiluminescence

While both OH PLIF and chemiluminescence probe the reaction field of the flow, there are differences in the data generated by each technique. Figure 7 shows a simultaneously recorded PLIF (a) and chemiluminescence (b) image from case (A). This OH PLIF image (a) has not been corrected for laser sheet non-uniformity so that comparison can be made between the emission induced by the laser and background chemiluminescence emission. Near the bottom of the frame the vertical location where the laser sheet terminates is marked. Above this point and along the leading front, where a PLIF signal is generated, the emission is 2.5-7 times more intense than the chemiluminescence signal below. Due to the large amount of background chemiluminescence that makes it through the spectral filter and is integrated over the 20 ns intensifier gate, it is impossible to determine if any of the emission that is more than 3-4 mm behind the front is OH PLIF. Nevertheless, the OH PLIF signal along the front is identifiable by the distinct edges it produces. Note that the strong background chemiluminescence was only observed for the methane fueled case (A). Figure 8 shows an image of a hydrogen fueled detonation and below the laser sheet location very little emission is produced.

There are a few features made visible through the use of OH PLIF (Fig. 7a) that are otherwise lost in the chemiluminescence image (Fig. 7b). Both frames show two triple points (i and ii) that are moving towards each other. Along the high-speed shocks attached to each triple-point there are fine corrugations in the PLIF that are likely associated with the large ranges of scales that manifest in highly unstable mixtures [10]. However, in the chemiluminescence the high-speed shocks appear smooth and do not resolve small-scale details due to the inherent path integration of the technique.

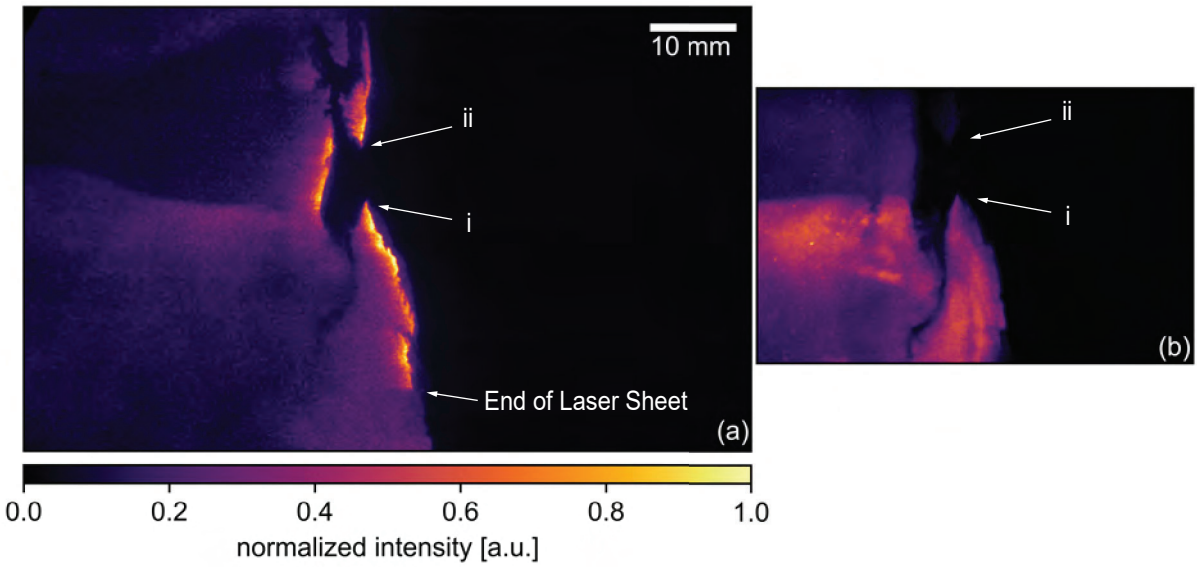

Fig. 7 Uncorrected OH PLIF (a) and chemiluminescence (b) of a methane fueled detonation (case A). The images were obtained simultaneously at t = 14.8μs (frame g in Fig. 9).

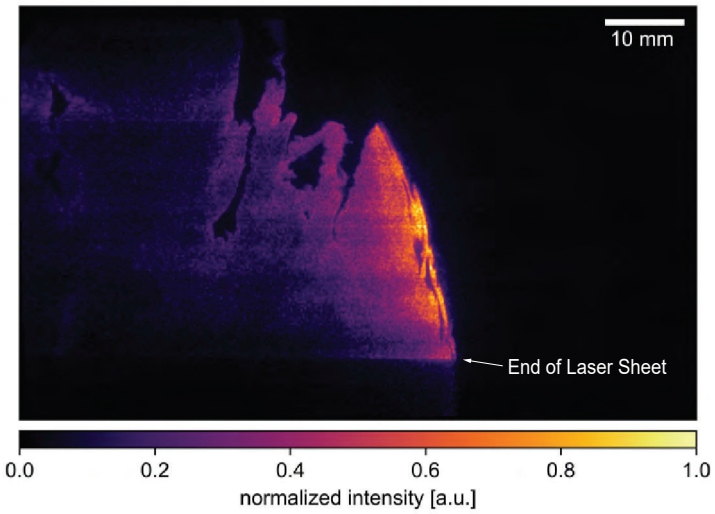

Fig. 8 Uncorrected OH PLIF image of hydrogen fueled detonation.

B. Asymmetric vortex development

The images captured for case (A) resolve the asymmetric collision of two transverse waves. A time series of the schlieren imgaes is shown in Figure 9. Note that the apparent "double" leading shock, which is particularly evident in frames a-c (feature i), is caused by the wave moving across the depth direction of the channel. At the beginning of the case a triple-point structure (ii) is moving up from the bottom of the frame. The transverse wave associated with this triple-point is strong, based on its definition in the schlieren and because in the chemiluminescence images (not shown) it is reactive. Moving down from the top of the frame is another triple-point structure (iv). The associated transverse wave (v) is weak and only creates a small disturbance in the schlieren. In frame (h) the transverse wave collision process begins (vi) and a new high-speed shock (vii) develops in the subsequent frames. Due to the mismatch in strength of the

transverse waves, the high-speed shock preferentially expands upward.

Growing out of the transverse wave collision are two small-scale vortical flow structures known as a forward and reverse jet [38]. Vortex pairs are generated when transverse waves meet and the fluid between them is forced forward and backwards along the symmetry axis. In frame (j) the reverse jet (viii) begins to form and most prominently appears in frame (m). Due to the asymmetry at the point of collision, the forward jet only produces one side of the vortex pair (ix), which can been developing from frame (k) onward and is labeled in frame (l). The forward jet sits right behind the high-speed shock. These vortices also serve to induce reaction through turbulent mixing, which becomes visible with the OH PLIF imaging. Figure 10 overlays the PLIF field with the schlieren frame (j) and (m) of Fig. 9. As the reverse jet (viii) begins protruding beyond the shear layer in Fig. 10a, the reaction field is contained within and remains so in frame (b) once both lobes of the vortex pair are resolvable. The high-intensity PLIF signal within the forward jet (ix) of frame (b) takes the shape of the vortex, while the surrounding fluid behind the high-speed shock remains unreacted. These vortices support a turbulent mode of combustion within the detonation structure.

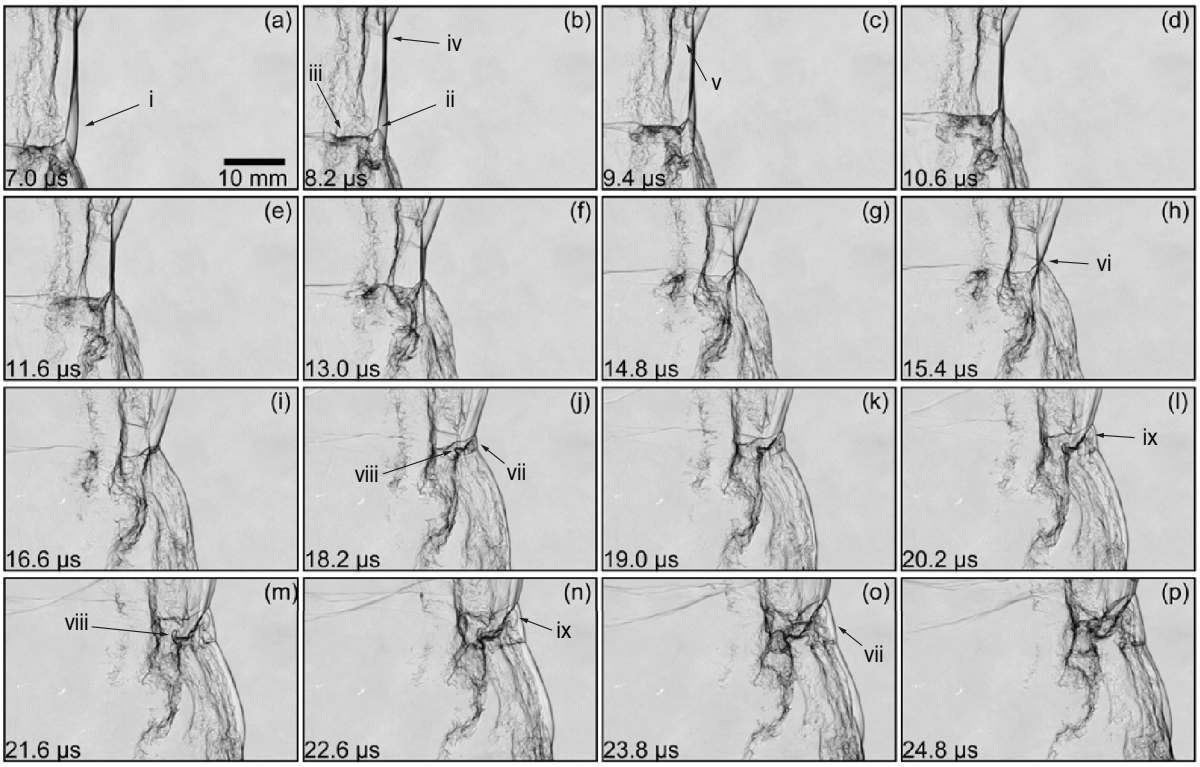

Fig. 9 Select schlieren images of the methane case (A).

C. Transverse Wave Collision

Case (B), the first of the hydrogen cases, like case (A) captures a transverse wave collision process. Four frames that show the evolution of the process are provided in Figure 11. The left column contains just the schlieren images and in the right column the schlieren and OH PLIF frames are overlaid. Before the transverse wave collision (frames a and b), the high-speed shocks (i and ii) appear smooth and uniform in both the schlieren and PLIF. This is in contrast to case (A) (Fig. 9), where the schlieren field is wrinkled and the PLIF is segmented behind the high-speed shock. This difference in appearance is a result of the hydrogen mixture being less unstable than the methane one in case (A) and not supporting the cellular substructure that manifests over a wide range of spatial scales. The non-dimensional activation energy θ is one value used to quantify instability and for case (B) it is two times less than case (A) (see Table 1).

Also present in these OH PLIF images are isolated vertical running strips of OH PLIF signal, such as (iii) in frame (d). Like the "double front" seen in the schlieren of case (A), these strips are caused by the wave moving across the depth of the channel and intersecting the laser sheet at an angle. This effect was previously observed and discussed by Pintgen *et al.* [39].

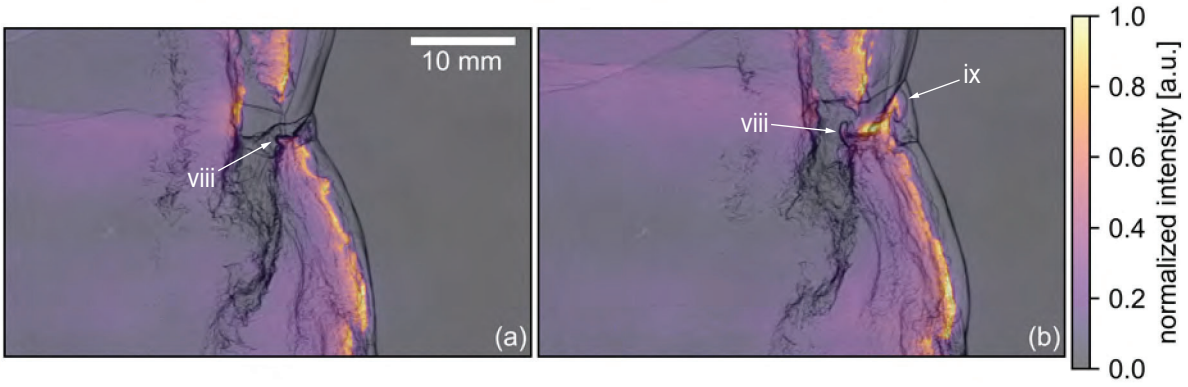

Fig. 10 Overlay of correct PLIF and schlieren showing reaction within developing vortices following transverse wave collision. Frames (a) and (b) of this figure correspond to frames (j) and (m) of Fig. 9, respectively.

Between the high-speed shock (i) and transverse wave exits a shear layer that separates the gases processed by each wave. This feature is labeled as (v) in frames (a-d). In the schlieren, the shear layer exhibits vortices due to a Kelvin-Helmholtz instability induced by the different speed, parallel moving flows. On the high-speed shock side of the shear layer, the OH PLIF signal conforms well to the contours in the schlieren. On the downstream side of (v) there is no OH PLIF signal. This visualization highlights the role of the shear layer in mixing combustion products and unreacted gases.

In frame (e), which occurs immediately after the transverse wave collision, the appearance of the new high-speed shock is obscured in the schlieren by the out of plane motion of the wave. However, in frame (f) the reaction induced behind the high-speed shock (vi) clearly protrudes and is directly attached to the leading shock. Behind this newly formed detonation head there is a "shadow " (vii) in the downstream region of the OH PLIF field. A large amount of the incident laser energy is absorbed by (vi) and so although the mixture composition and state in the downstream portion of the image and within the "shadow " is likely similar to the brighter regions surrounding it, less OH PLIF signal is produced.

D. Unreacted Gas Pockets

Figure 12 shows a time series of the OH PLIF images captured for case (C). In the first frame (a) we observe the reaction zone behind a decaying low-speed (i) and high-speed (ii) shock. In the subsequent frames the high-speed shock moves upward until a transverse wave collision occurs at some time between frames (c) and (d). In frame (d), a newly formed high-speed shock (iii) is observed at the top of the image. For the remainder of the case the leading front continues forward without need of detailed narration. The features we are interested in discussing with this case are the pockets of unreacted gas that convect downstream of the leading front.

From frames (a) - (c) unreacted gas enters behind the leading front by passing through the low-speed shock (iv) and then the transverse wave (v). Because the schlieren field of view does not overlap with this region of the PLIF image, the approximate location of these shocks is sketched in frame (b). The gas collects in the region downstream of shear layer (vi), as with case (b). Once transverse waves collide in frame (d), the entrance to this pocket of unreacted gas is closed off and it separates from the front. By the time frame (d) is recorded, the pocket is now visible in the schlieren and Figure 13a overlays the schlieren and OH PLIF for frame (d). Shear layer (vi) is apparent in the schlieren and serves as the upstream bound for the pocket. The pocket size decreases as it convects downstream from the front. In frame (g), which is also overlaid with schlieren in Fig. 13b, there is an increases in OH PLIF emission from the periphery of the pocket and along the shear layer. Further downstream, another region of increased emission (vii) enters the field of view.

It is likely that the increased emission seen at (vi) and (vii) is a result of the pockets of unreacted gas deflagrativly burning. This event has been observed in numerous numerical studies, but experimental evidence has been lacking. In our previous work [15], which utilized chemiluminescence to probe the reaction field, we theorized that the emission from these pockets would be too weak to pick up with chemiluminescence imaging. However, Kiyanda and Higgins [11] did observe increased emission in their chemiluminescence measurements. Further study is needed across a wider range of mixtures and to validate the observations made here.

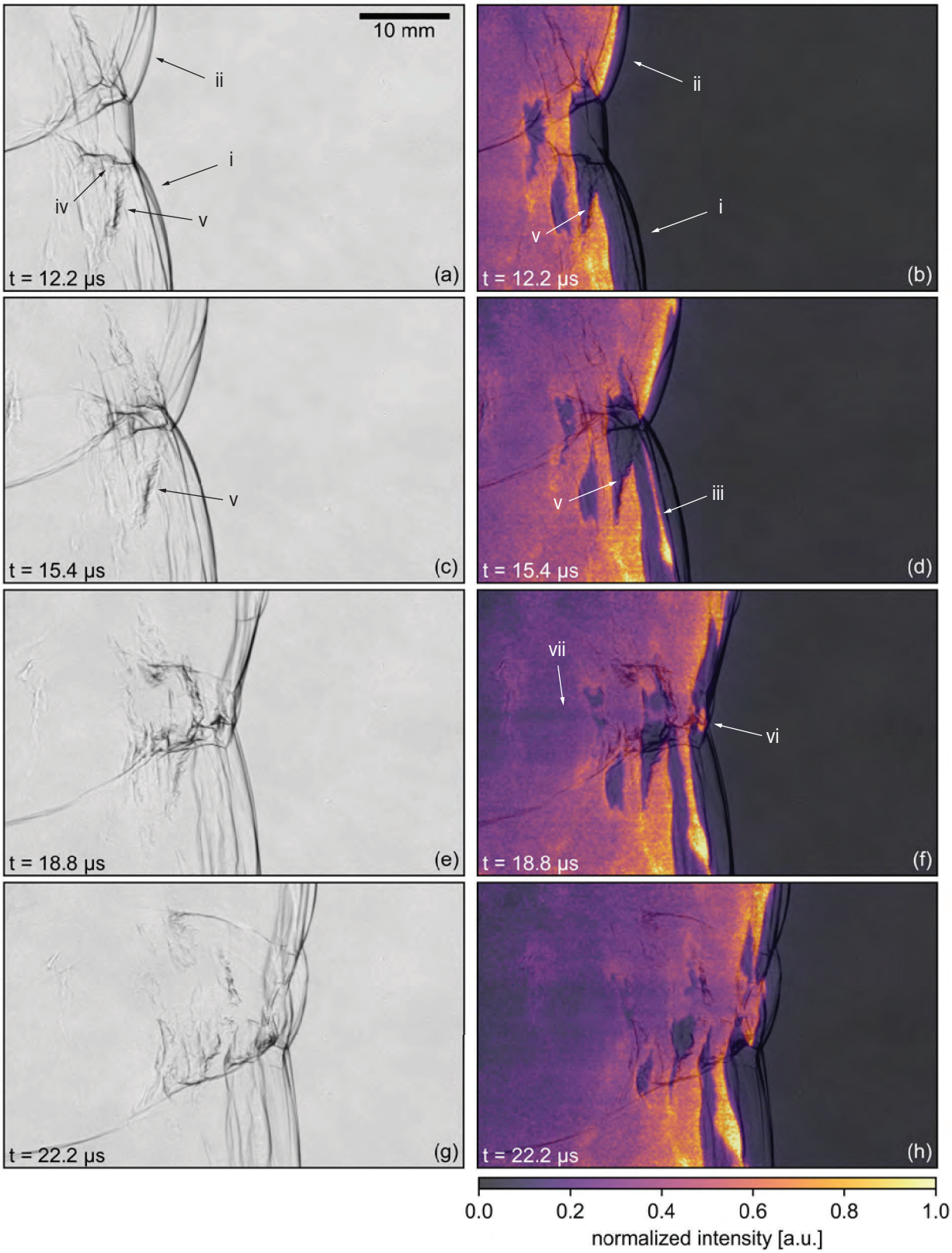

Fig. 11 Isolated schlieren (a,c,e,g) and schlieren-PLIF overlays (b,d,f,h) for a mixture of $2H_2$-O_2-$3.9N_2$ (case B).

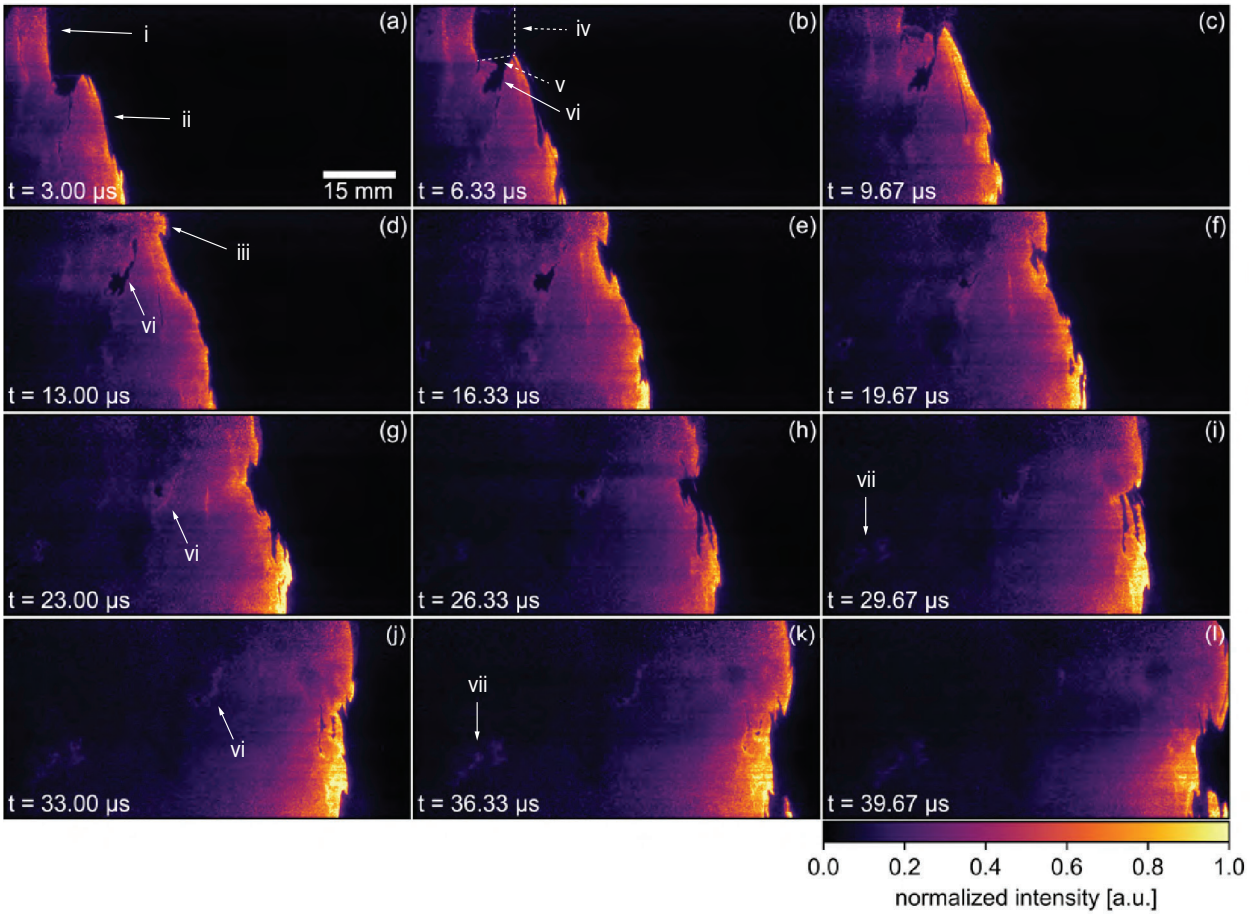

Fig. 12 Time-series of corrected OH PLIF images for a mixture of $2H_2$-O_2-$3.9N_2$ (case C).

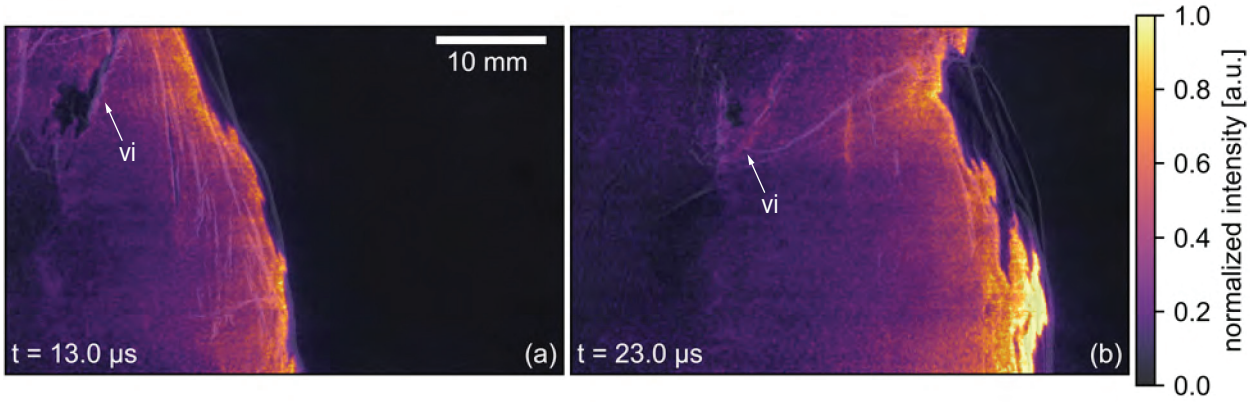

Fig. 13 Overlaid schlieren and OH PLIF for two select frames from case (C). Sub-figures (a) and (b) correspond to frames (d) and (g) in Fig. 12, respectively.

IV. Conclusion

Time-resolved images of the reaction field of methane-oxygen-nitrogen and hydrogen-oxygen-nitrogen detonations were captured using 300 kHz OH PLIF. When compared with chemiluminescence, the OH PLIF revealed small-scale reaction structure along the leading front of a highly-unstable wave that was obscured by the path integrated technique. By overlaying PLIF with select frames of simultaneously obtained 5 MHz schlieren, shear layers were identified that

bound distinct regions of OH emission in downstream portions of the flow and served as mixing locations for combustion products and unburned reactants. Vortex structures generated by transverse wave collision were observed to locally contain and support reaction. Finally, pockets of unreacted gas were observed burning as far as 78 mm downstream of the leading front.

Acknowledgments

This work was supported by U.S. Air Force Office of Scientific Research grant FA9550-21-1-0013 (PO: Dr. Chiping Li). Mark D. Frederick acknowledges support from the National Science Foundation Graduate Research Fellowship Program under Grant No. DGE-1333468. The high-speed imaging equipment was purchased with DURIP grants FA9550-16-1-0534, FA9550-20-1-0226, and FA9550-23-1-0403 (PO: Dr. Chiping Li). The authors are grateful to Hadland Imaging for use of the second Shimadzu HPV-X2.

References

[1] White, D. R., "Turbulent structure of gaseous detonation," *Physics of Fluids*, Vol. 4, 1961, pp. 465–480. https://doi.org/10.1063/1.1706350, URL https://doi.org/10.1063/1.1706350.

[2] Denisov, Y. N., and Troshin, Y. K., "Pulsating and spinning detonation of gaseous mixtures in tubes," *Dokl. Akad. Nauk SSSR*, Vol. 125, 1959, p. 110.

[3] Duff, R., "Investigation of spinning detonation and detonation stability," *Physics of Fluids*, Vol. 4, 1961. https://doi.org/https://doi.org/10.1063/1.1706235.

[4] Metrow, C., Gray, S., and Ciccarelli, G., "Detonation propagation through a nonuniform layer of hydrogen-oxygen in a narrow channel," *International Journal of Hydrogen Energy*, Vol. 46, 2021. https://doi.org/10.1016/j.ijhydene.2021.03.221.

[5] Schumaker, S. A., Knisely, A. M., Hoke, J. L., and Rein, K. D., "Methane-oxygen detonation characteristics at elevated pre-detonation pressures," *Proceedings of the Combustion Institute*, Vol. 38, No. 3, 2021, pp. 3623–3632. https://doi.org/10.1016/j.proci.2020.07.066.

[6] Voitsekhovskii, B. V., Mitrofanov, V. V., and Topchiyan, M. Y., "The structure of a detonation front in gases," Tech. rep., 1963.

[7] Strehlow, R. A., and Crooker, A. J., "The structure of marginal detonation waves," *Acta Astronautica*, Vol. 1, No. 3-4, 1974, pp. 303–315. https://doi.org/10.1016/0094-5765(74)90100-3.

[8] Akbar, R., "MACH REFLECTION OF GASEOUS DETONATIONS," Ph.D. thesis, Rensselaer Polytechnic Institute, 1997.

[9] Takai, R., Yoneda, K., and Hikita, T., "Study of detonation wave structure," *Symposium (International) on Combustion*, Vol. 15, No. 1, 1975, pp. 69–78. https://doi.org/10.1016/S0082-0784(75)80285-2.

[10] Austin, J., Pintgen, F., and Shepherd, J., "Reaction zones in highly unstable detonations," *Proceedings of the Combustion Institute*, Vol. 30, No. 2, 2005, pp. 1849–1857. https://doi.org/10.1016/j.proci.2004.08.157.

[11] Kiyanda, C. B., and Higgins, A. J., "Photographic investigation into the mechanism of combustion in irregular detonation waves," *Shock Waves*, Vol. 23, 2013, pp. 115–130. https://doi.org/10.1007/s00193-012-0413-8.

[12] Bhattacharjee, R. R., "Experimental Investigation of Detonation Re-initiation Mechanisms Following a Mach Reflection of a Quenched Detonation," Ph.D. thesis, Ottawa-Carleton Institute for Mechanical and Aerospace Engineering, 2013. URL http://www.ruor.uottawa.ca/handle/10393/24933.

[13] Maley, L., Bhattacharjee, R., Lau-Chapdelaine, S. M., and Radulescu, M. I., "Influence of hydrodynamic instabilities on the propagation mechanism of fast flames," *Proceedings of the Combustion Institute*, Vol. 35, 2015, pp. 2117–2126. https://doi.org/10.1016/j.proci.2014.06.134.

[14] Kellenberger, M., and Ciccarelli, G., "Simultaneous schlieren photography and soot foil in the study of detonation phenomena," *Experiments in Fluids*, Vol. 58, No. 10, 2017, pp. 1–13. https://doi.org/10.1007/s00348-017-2420-0.

[15] Frederick, M. D., Gejji, R. M., Shepherd, J. E., and Slabaugh, C. D., "Time-resolved imaging of the cellular structure of methane and natural gas detonations," *Shock Waves*, Vol. 32, 2022, pp. 337–351. https://doi.org/10.1007/s00193-022-01080-8.

[16] Zangene, F., Xiao, Q., and Radulescu, M., "Critical diffraction of irregular structure detonations and their predictability from experimentally obtained Dκ data," *Proceedings of the Combustion Institute*, Vol. 39, No. 3, 2023, pp. 2935–2944. https://doi.org/10.1016/j.proci.2022.11.004.

[17] Frederick, M. D., Gejji, R. M., Shepherd, J. E., and Slabaugh, C. D., "Statistical analysis of detonation wave structure," *Proceedings of the Combustion Institute*, Vol. 39, 2023, pp. 2847–2854. https://doi.org/10.1016/J.PROCI.2022.08.054.

[18] Campbell, C., and Woodhead, W., "The Ignition of Gases by an Explosive-Wave. Part I. Carbon Monoxide and Hydrogen Mixtures," *Journal of the Chemical Society*, 1926.

[19] Schott, G., "Observations of the structure of spinning detonation," *Physics of Fluids*, Vol. 8, No. 5, 1965, p. 850.

[20] Radulescu, M. I., Sharpe, G. J., Lee, J. H., Kiyanda, C. B., Higgins, A. J., and Hanson, R. K., "The ignition mechanism in irregular structure gaseous detonations," *Proceedings of the Combustion Institute*, Vol. 30, 2005, pp. 1859–1868. https://doi.org/10.1016/J.PROCI.2004.08.047.

[21] Pintgen, F., and Shepherd, J. E., "Detonation diffraction in gases," *Combustion and Flame*, Vol. 156, 2009, pp. 665–677. https://doi.org/10.1016/j.combustflame.2008.09.008.

[22] Frederick, M. D., Gejji, R. M., Shepherd, J. E., and Slabaugh, C. D., "Transverse Detonation Waves in Near-Limit Detonations," *AIAA SCITECH 2023 Forum*, American Institute of Aeronautics and Astronautics, 2023. https://doi.org/10.2514/6.2023-1874, URL https://arc.aiaa.org/doi/10.2514/6.2023-1874.

[23] Austin, J. M., "The role of instability in gaseous detonation," Ph.D. thesis, California Institute of Technology, 2003. https://doi.org/10.7907/X7YH-T687.

[24] Mével, R., Davidenko, D., Austin, J. M., Pintgen, F., and Shepherd, J. E., "Application of a Laser Induced Fluorescence Model to the Numerical Simulation of Detonation Waves in Hydrogen-Oxygen-Diluent Mixtures," *International J of Hydrogen Energy*, Vol. 30, 2014, pp. 6044–6060. https://doi.org/10.1016/j.ijhydene.2014.01.182.

[25] Pintgen, F., "Laser-Optical Visualization of Detonation Structures," Ph.D. thesis, Technische Universitat Munchen, 2000.

[26] Rojas Chavez, S. B., Chatelain, K. P., Guiberti, T. F., Mével, R., and Lacoste, D. A., "Effect of the excitation line on hydroxyl radical imaging by laser induced fluorescence in hydrogen detonations," *Combustion and Flame*, Vol. 229, 2021. https://doi.org/10.1016/j.combustflame.2021.111399.

[27] Grib, S. W., Fugger, C. A., Hsu, P. S., Jiang, N., Roy, S., and Schumaker, S. A., "Two-dimensional temperature in a detonation channel using two-color OH planar laser-induced fluorescence thermometry," *Combustion and Flame*, Vol. 228, 2021, pp. 259–276. https://doi.org/10.1016/j.combustflame.2021.02.002.

[28] Rojas Chavez, S. B., Chatelain, K. P., and Lacoste, D. A., "Two-dimensional visualization of induction zone in hydrogen detonations," *Combustion and Flame*, Vol. 255, 2023. https://doi.org/10.1016/j.combustflame.2023.112905.

[29] Jackson, S. I., Austin, J. M., and Shepherd, J. E., "Planar detonation wave initiation in large-aspect-ratio channels," *AIAA Journal*, Vol. 44, No. 10, 2006, pp. 2422–2425. https://doi.org/10.2514/1.21581.

[30] Frederick, M. D., Gejji, R. M., Shepherd, J. E., and Slabaugh, C. D., "Preliminary Results from Narrow Channel Facility Experiments at Purdue University," *AIAA Propulsion and Energy Forum*, 2019, pp. 1–8. https://doi.org/10.2514/6.2019-4218.

[31] Hsu, P. S., Slipchenko, M. N., Jiang, N., Fugger, C. A., Webb, A. M., Athmanathan, V., Meyer, T. R., and Roy, S., "Megahertz-rate OH planar laser-induced fluorescence imaging in a rotating detonation combustor," *Optics Letters*, Vol. 45, No. 20, 2020, p. 5776. https://doi.org/10.1364/OL.403199.

[32] Luque, J., and Crosley, D., "LIFBASE: Database and Spectral Simulation Program," , 1999. URL https://www.sri.com/platform/lifbase-spectroscopy-tool/.

[33] Hanson, R. K., Spearrin, R. M., and Goldenstein, C. S., "Spectroscopy and optical diagnostics for gases," *Spectroscopy and Optical Diagnostics for Gases*, Springer Cham, 2016, Chap. 8, pp. 131–148. https://doi.org/10.1007/9783319232522.

[34] Rea, E. C., Chang, A. Y., and Hanson, R. K., "Collisional Broadening of the $A^2\Sigma^+ \leftarrow X^2\Pi(0,0)$ Band of OH by H_2O and CO_2 in Atmospheric-Pressure Flames," *Journal of Quantitative Spectroscopy and Radiative Transfer*, Vol. 41, No. I, 1989, pp. 29–42. https://doi.org/10.1016/0022-4073(89)90018-6.

[35] Kessler, W. J., Allen, M. G., and Davis, S. J., "Rotationon Level-Dependent Collisional Broadending and Line Shift of the $A^2\Sigma^+ - X^2\Pi$ Band of OH in Hydrogen-Air Combsution Gases," *Journal of Quantum Spectroscopy and Radiative Transfer*, Vol. 49, No. 2, 1993, p. 107. https://doi.org/10.1016/0022-4073(93)90051-I.

[36] Shepherd, J., "Shock and Detonation Toolbox," , 2018. URL https://shepherd.caltech.edu/EDL/PublicResources/sdt/.

[37] Smith, G. P., Golden, D. M., Frenklach, M., Moriarty, M. W., Eiteneer, B., Goldenberg, M., Bowman, C. T., Hanson, R. K., Song, S., Gardiner, W. C., Lissianski, V. V., and Qin, Z., "GRI-Mech," , Jul. 1999. URL www.me.berkeley.edu/gri_mech/.

[38] Subbotin, V., "Collision of transverse detonation waves in gases," *Combustion, Explosion, and Shock Waves*, Vol. 11, No. 3, 1975, pp. 411–414. https://doi.org/10.1007/BF00740553.

[39] Pintgen, F., Eckett, C., Austin, J., and Shepherd, J., "Direct observations of reaction zone structure in propagating detonations," *Combustion and Flame*, Vol. 133, No. 3, 2003, pp. 211–229. https://doi.org/10.1016/S0010-2180(02)00458-3.